Heliyon 10 (2024) e36898

Contents lists available at ScienceDirect

Heliyon

journal homepage: www.cell.com/heliyon

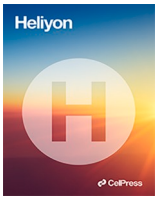

Research article

A clinical prognostic model related to T cells based on machine learning for predicting the prognosis and immune response of ovarian cancer

Qiwang Lin [a,b,c,1], Weixu Ma [d,1], Mengchang Xu [e], Zijin Xu [b], Jing Wang [b], Zhu Liang [b], Lin Zhu [b], Menglu Wu [b], Jiejun Luo [b], Haiying Liu [b,*], Jianqiao Liu [b,**], Yunfeng Jin [a,c,***]

[a] Department of Obstetrics and Gynecology, Affiliated Hospital of Nantong University, Nantong, Jiangsu Province, China
[b] Department of Obstetrics and Gynecology, Center for Reproductive Medicine, Guangdong Provincial Key Laboratory of Major Obstetric Diseases, Guangdong Provincial Clinical Research Center for Obstetrics and Gynecology, Guangdong Hong Kong Macao Greater Bay Area Higher Education Joint Laboratory of Maternal-Fetal Medicine, The Third Affiliated Hospital, Guangzhou Medical University, Guangzhou, China
[c] Department of Gynecology, Obstetrics & Gynecology Hospital, Fudan University, Shanghai, China
[d] Department of Obstetrics and Gynecology, Guangzhou Women and Children's Medical Center, Guangzhou, China
[e] Hunan Provincial Key Laboratory of the Research and Development of Novel Pharmaceutical Preparations, Changsha Medical University, Provincial First-class Applied Discipline (pharmacy), Changsha, China

ARTICLE INFO

Keywords:
Ovarian cancer
Single-cell analysis
Machine learning
Clinical prognostic model
PFN1

ABSTRACT

Background: Ovarian cancer (OV) is regarded as one of the most lethal malignancies affecting the female reproductive system, with individuals diagnosed with OV often facing a dismal prognosis due to resistance to chemotherapy and the presence of an immunosuppressive environment. T cells serve as a crucial mediator for immune surveillance and cancer elimination. This study aims to analyze the mechanism of T cell-associated markers in OV and create a prognostic model for clinical use in enhancing outcomes for OV patients.

Methods: Based on the single-cell dataset GSE184880, this study used single-cell data analysis to identify characteristic T cell subsets. Analysis of high dimensional weighted gene co-expression network analysis (hdWGCNA) is utilized to identify crucial gene modules along with their corresponding hub genes. A grand total of 113 predictive models were formed utilizing ten distinct machine learning algorithms along with the combination of the cancer genome atlas (TCGA)-OV dataset and the GSE140082 dataset. The most dependable clinical prognostic model was created utilizing the leave one out cross validation (LOOCV) framework. The validation process for the models was achieved by conducting survival curve analysis and receiver operating characteristic (ROC) analysis. The relationship between risk scores and immune cells was explored through the utilization of the Cibersort algorithm. Additionally, an analysis of drug sensitivity was carried out to anticipate chemotherapy responses across various risk groups. The genes implicated in the model were authenticated utilizing qRT-PCR, cell viability experiments, and EdU assay.

* Corresponding author.
** Corresponding author.
*** Corresponding author.
E-mail addresses: 2011683120@gzhmu.edu.cn (H. Liu), liujqssz@gzhmu.edu.cn (J. Liu), jinyunfeng@ntu.edu.cn (Y. Jin).
[1] These authors contributed equally.

https://doi.org/10.1016/j.heliyon.2024.e36898
Received 9 July 2024; Received in revised form 22 August 2024; Accepted 23 August 2024
Available online 24 August 2024

Results: This study developed a clinical prognostic model that includes ten risk genes. The results obtained from the training set of the study indicate that patients classified in the low-risk group experience a significant survival advantage compared to those in the high-risk group. The ROC analysis demonstrates that the model holds significant clinical utility. These results were verified using an independent dataset, strengthening the model's precision and dependability. The risk assessment provided by the model also serves as an independent prognostic factor for OV patients. The study also unveiled a noteworthy relationship between the risk scores calculated by the model and various immune cells, suggesting that the model may potentially serve as a valuable tool in forecasting responses to both immune therapy and chemotherapy in ovarian cancer patients. Notably, experimental evidence suggests that PFN1, one of the genes included in the model, is upregulated in human OV cell lines and has the capacity to promote cancer progression in in vitro models.
Conclusion: We have created an accurate and dependable clinical prognostic model for OV capable of predicting clinical outcomes and categorizing patients. This model effectively forecasts responses to both immune therapy and chemotherapy. By regulating the immune microenvironment and targeting the key gene PFN1, it may improve the prognosis for high-risk patients.

1. Introduction

Ovarian cancer (OV) is a highly lethal disease that impacts the female reproductive system. While the overall occurrence of OV has stayed fairly consistent, its fatality rate is the greatest among gynecological cancers. The primary reason for this high fatality rate is the late detection of the majority of cases [1]. Diagnosing OV in its early stages poses a challenge because there are no obvious initial clinical symptoms and the ovaries are located in a concealed position. The conventional screening methods for OV include ultrasound examination and tumor marker detection (such as CA-125), which have limitations in sensitivity and specificity [2]. At the initial diagnosis, over 70 % of people with OV are already in an advanced stage, resulting in a 5-year survival rate of only 35 % [3,4]. Standard treatments for OV encompass surgery, chemotherapy, immunotherapy, and targeted therapy. However, due to significant tumor heterogeneity, a complex tumor microenvironment, and the development of resistance to these treatments, the majority of OV patients eventually face recurrence and disease progression [5–7]. Hence, it remains crucial to create effective clinical prognostic models and detect fresh biomarkers associated with the onset, progression, and outcome of OV.

In OV, the complex interaction between malignant tumors and the tumor microenvironment (TME) plays a crucial role in cancer progression, metastasis, and the development of resistance to various therapies [8,9]. The prognosis of patients with tumors and their response to immunotherapies are profoundly affected by the infiltration and phenotypic diversity of immune cells, particularly T cells, within solid tumor tissues [10,11]. T cells, serving as key agents in immune surveillance and cancer elimination, play a pivotal role. Dysfunction or inadequate regulation of T cells within tumors can contribute to resistance against immunotherapy [12]. Previous research has shown that $CD4^+$ T cells can either directly kill tumor cells via cell lysis or modulate the TME indirectly to target cancer cells [13,14]. In breast cancer, a model based on CD8 T cells is significantly associated with clinical outcomes and the sensitivity to treatment [15]. Notably, the infiltration of $CD8^+$ cytotoxic T cells is frequently associated with improved survival, indicating that T cells may exert a suppressive influence on OV progression [16]. Another study also showed that in most immunotherapy environments, CD8+T lymphocytes can eradicate OV cells and are associated with good patient survival [17]. Hence, understanding the patterns of expression for T cell markers in OV and creating a prognostic model could enhance the overall treatment results for patients with OV.

With the accumulation of multi omics data and optimization of algorithms, OV research is entering a data-driven new era. Bioinformatics plays a crucial role in deciphering the complex biological network of diseases by integrating multiple omics data such as genomes, transcriptomics, proteomics, and metabolomics [18]. Bioinformatics offers tools for constructing analytical models and biological networks within the realm of systems biology, thereby assisting researchers in comprehending the complexity and dynamic processes of biological systems. Furthermore, bioinformatics facilitates the analysis of the relationship between an individual's genetic background and disease risk, providing foundational support for personalized treatment. Through the analysis of these data, future studies may uncover additional biomarkers, prognostic factors, and potential therapeutic targets to advance precision medicine for OV [19]. Single-cell RNA sequencing is a revolutionary technology that has significantly enhanced our understanding of the diversity and behavior of cellular transcriptomes across various organisms. Ding et al. demonstrated the heterogeneity of fibroblast subpopulations within the ovarian cancer tissue microenvironment through comprehensive single-cell analysis [20]. Similarly, Zhao et al. identified the critical role of IL4I1 in promoting ovarian cancer progression using single-cell analysis [21]. In this study, T cell related marker genes in OV were identified using single-cell analysis. Furthermore, a clinical prognosis model was developed utilizing machine learning algorithms with data from the TCGA dataset and the GEO dataset (GSE140082). This model is anticipated to effectively categorize OV patients, pinpoint specific subgroups that can benefit from immunotherapy, and ultimately enhance the overall clinical prognosis for individuals with OV.

2. Materials and methods

2.1. Data acquisition and processing

Data analysis was conducted using information from the cancer genome atlas (TCGA) database (TCGA-OV) and GEO database (GSE140082). TCGA-OV, as the training set, contains mRNA expression and related clinical information of 381 OV tissues. We obtained information from the GTEx database Obtained mRNA expression information from 88 normal samples to increase the number of normal samples. Batch effects were removed using the SVA and LIMMA R packages [22,23]. As a validation set, GSE140082 contains mRNA expression and related clinical information from 380 OV tissues. Furthermore, somatic and copy number variation data for OV patients were retrieved from the TCGA database. Single-cell sequencing data for human OV tissue were sourced from the GEO database (GSE184880). Within the GSE184880 dataset, sequencing details for 7 OV tissues and 5 normal ovarian tissues were included.

2.2. Single cell data processing

The Seurat R package was utilized for generating Seurat objects from scRNA seq data [24,25]. The first step involved implementing quality control measures to remove cells that did not meet certain criteria, such as having fewer than 200 expressed genes, more than 2500 expressed genes, or a mitochondrial gene content exceeding 10 %. Following this, principal component analysis was conducted on the top 2000 most variable genes, with the selection of 10 principal components for reducing dimensionality and clustering. To address sample integration and batch effects, the harmony function was employed. Following the outcomes of Harmony, the RunUMAP function was employed for Unified Manifold Approximation Projection (UMAP) dimensionality reduction, while the FindNeighbors and FindClusters functions were utilized for neighborhood search and clustering analysis to understand the data structure. Lastly, the identification function was deployed to acquire the clustering labels for the samples.

2.3. High dimensional WGCNA (hdWGCNA) analysis

High-dimensional WGCNA (hdWGCNA) is a thorough methodological framework designed to deduce, assess, and understand gene co-expression networks within high-dimensional transcriptomic datasets [26]. The hdWGCNA method was employed to establish scale-free networks at the individual cellular level. This was achieved using the R package 'hdWGCNA,' which was instrumental in optimizing network connectivity by setting the scale-free topology model threshold above 0.85 and selecting a soft threshold of 6. To illustrate the similarity in gene expression, Pearson correlation coefficients were utilized to generate a topological overlap matrix (TOM). Following this, a clustering tree was constructed using the 'PlotDendrogram' function, grouping genes into distinct modules. Module Eigengenes were then used to analyze the correlation between these modules and cell clusters, with the aim of identifying the most pertinent ones. From the various modules, seven were selected for a more focused examination. Within these modules, the top 100 genes were identified and designated as hub genes. To further understand the functions of these hub genes, a functional enrichment analysis was carried out using Gene Ontology (GO) and Kyoto Encyclopedia of Genes and Genomes (KEGG), facilitated by the 'clusterProfiler' package.

2.4. Differential expression analysis

The expression levels of hub genes in the TCGA-OV group were gathered and analyzed for differential expression between ovarian cancer (OV) and normal groups using the 'limma' package in R. The threshold was logfc$>$1 or logfc < -1, $P < 0.05$.

2.5. A comprehensive machine learning algorithm was used to construct a clinical prognostic model related to T cells

Through the utilization of differentially expressed genes (DEGs), a univariate Cox regression analysis was performed to pinpoint significant genes with prognostic importance. To establish a clinical prognostic model that boasts both precision and reliability, We integrated multiple machine learning algorithms and explored various combinations of these algorithms. The algorithms used include Random Forest (RF), Extreme Gradient Boosting (XGBoost), Elastic Net (Enet), Least Absolute Shrinkage and Selection Operator (Lasso), Ridge, Stepglm, glmBoost, Linear Discriminant Analysis (LDA), Gradient Boosting Machine (GBM), Support Vector Machine (SVM), and Naive Bayes. The optimal model is acknowledged as the model that produces the highest average C-index across all datasets.

2.6. Evaluation and validation of clinical prognostic models

The TCGA-OV patient cohort was separated into two groups: high-risk and low-risk, according to the calculated risk score from the model. To compare the survival rates between these groups, Kaplan-Meier analysis was utilized. Heatmaps depicted gene expression levels which were instrumental in developing the prognostic models for clinical outcomes in both groups. The model's performance was measured using the area under the ROC curve (AUC). To identify risk factors affecting OV clinical outcomes, both univariate and multivariate Cox regression analyses were performed, taking into account the risk score along with other clinical characteristics. Lastly, the predictive capability of the clinical prognostic model was validated through analysis using a separate validation group.

2.7. Correlation analysis between risk score and clinical features, immune microenvironment, and somatic mutations

The research examined the relationship between the risk score of the model and various clinical traits. Furthermore, the CIBERSPORT algorithm was employed to assess the ratios of infiltrating immune cells in ovarian cancer, and to investigate the association between the risk score and immune cell infiltration. The genetic profile was displayed utilizing the software 'maftools'. An analysis of the genetic terrain between low-risk and high-risk classifications was carried out utilizing the R package 'maftools' [27].

2.8. Drug sensitivity analysis

To forecast chemical sensitivity among high and low-risk groups, the Cancer Drug Sensitivity Genomics (GDSC) database, along with the pRRophetic R software package, was employed. We utilized a ridge regression model and implemented ten-fold cross-validation to estimate the half maximal inhibitory concentration (IC50) values [28,29].

2.9. Cell culture and transient transfection

The IOSE80 cell line, derived from human ovarian epithelial cells, as well as the A2780 and HEY cell lines, both originating from human OV cells, were obtained from Beijing Bena Biotechnology Co. in Beijing, China. Subsequent cultivation of these cell lines was carried out in DEME F-12 medium. The transfection procedures were conducted with Lipofectamine 2000 (Invitrogen, Thermo Fisher, USA) using negative control (NC) and PFN1 siRNA (Sagon, China).

Gene	Target sequences (5′-3′)
si-PFN1#1	TGGCAAAGACCGGTCAAGTTTTT
si-PFN1#2	CTGAGTCTTACCCTTCCTTTAGC

2.10. Quantitative real-time polymerase chain reaction (qRT-PCR)

RNA extraction was conducted on A2780 and HEY cell lines using TRIzol solution (Thermo Fisher, USA). After that, cDNA synthesis was performed with HiScript II SuperMix (Vazyme, China) using 500 ng of RNA. Subsequent to this, qRT-PCR was carried out on an ABI 7500 System (Thermo Fisher, USA) with SYBR Green Master Mix. The PCR amplification conditions consisted of 45 cycles: 10 min at 94 °C, then 10 s at 94 °C and 45 s at 60 °C. The internal reference used was GAPDH. The sequences of the primer pairs for the targeted genes can be found below.

Table 1. The sequences of the primer pairs for the targeted genes.

Gene	Forward primer sequence (5′-3′)	Reverse primer sequence (5′-3′)
TGOLN2	GGAGAGCAGCCACTTCTTTGCA	CCAAACGTTGGTAGTCACTGGC
NBL1	TCCACAGAGTCCCTGGTTCACT	GCTACAGTGCAGGATCTTCTCC
ARID1B	CCAGTCAACTGGCAGCAATTCC	CACTCACATCTGAGAATGGGTCG
ISG20	ACACGTCCACTGACAGGCTGTT	ATCTTCCACCGAGCTGTGTCCA
KRAS	CAGTAGACACAAAACAGGCTCAG	TGTCGGATCTCCCTCACCAATG
CLIC3	CATCCTGCTCTATGACAGCGAC	GGTGTTGGACTCCCTGTAACGA
ALOX5AP	AAGTGGAGCACGAAAGCAGGAC	AGACCAGAGCACAGCGAGGAAA
PFN1	CATCGTGGGCTACAAGGACTCG	CCAAGTGTCAGCCCATTCACGT
DNAJA1	GGTGAAGGAGACCAAGAACCAG	AGCCACACAGTGCTTCAACGAG
LASP1	CTTCGCCTCAAGCAACAGAGTG	TGTCTGCCACTACGCTGAAACC
P21	AGGTGGACCTGGAGACTCTCAG	TCCTCTTGGAGAAGATCAGCCG
BAX	TCAGGATGCGTCCACCAAGAAG	TGTGTCCACGGCGGCAATCATC
CDH1	GCCTCCTGAAAAGAGAGTGGAAG	TGGCAGTGTCTCTCCAAATCCG
CDH2	CCTCCAGAGTTTACTGCCATGAC	GTAGGATCTCCGCCACTGATTC
GAPDH	GTCTCCTCTGACTTCAACAGCG	ACCACCCTGTTGCTGTAGCCAA

2.11. Cell viability

Cell viability was measured by conducting the Cell Counting Kit-8 assay (Beyotime, China) in accordance with the instructions provided by the manufacturer. Various compounds were administered to the cells, which were then placed in 96-well plates with a cell density of 1 × 103 cells per well. At specified intervals, the CCK-8 solution was introduced and incubated for 2 h at 37 °C. Subsequently, the optical density (O.D) of 450 was determined using a microplate reader from BioTek (USA).

2.12. 5-Ethynyl-2′-deoxyuridine (EdU) assay

The EdU assay was conducted utilizing the BeyoClick™ EdU Cell Proliferation Kit featuring Alexa Fluor 594 (Biotek, Shanghai, China). Post-PBS rinse, the cells underwent a 2-h incubation period with the EdU solution, followed by DAPI staining to highlight the nuclei. Subsequent to washing, observations of the samples were made using an Olympus inverted microscope.

2.13. Statistical analysis

R software (version 4.3.3) is used for all statistical analysis and visualization. The Wilcoxon test is used to compare the differences between two groups. Survival analysis was conducted using univariate Cox regression analysis, while correlations were assessed using Pearson correlation analysis. P value < 0.05 has statistical significance.

3. Results

3.1. Single cell RNA sequencing analysis reveals cellular heterogeneity in OV tissues

The scRNA-seq dataset utilized in this research includes seven samples of ovarian cancer (OV) and five normal samples sourced from the GEO database. Following comprehensive quality assessment and clustering for dimensionality reduction, a total of 15 cell clusters were recognized and categorized into eight different cell types, demonstrating substantial diversity across various cell populations (Fig. 1A and B). In comparison to the normal samples, there was a marked rise in the proportion of T cell subgroups within the OV samples (Fig. 1C). Subsequently, an in-depth examination of the T cell subpopulations was carried out, revealing the presence of 14 distinct cell clusters. Of these clusters, 6 (specifically clusters 2, 5, 6, 8, 10, and 11) displayed significantly higher prevalence in OV samples than in normal samples. These particular clusters will be further explored within the context of ovarian cancer (Fig. 1D and E).

3.2. HdWGCNA algorithm identifies key modules

The hdWGCNA algorithm was utilized to elucidate the molecular characteristics of essential fibroblast modules. By creating a scale-

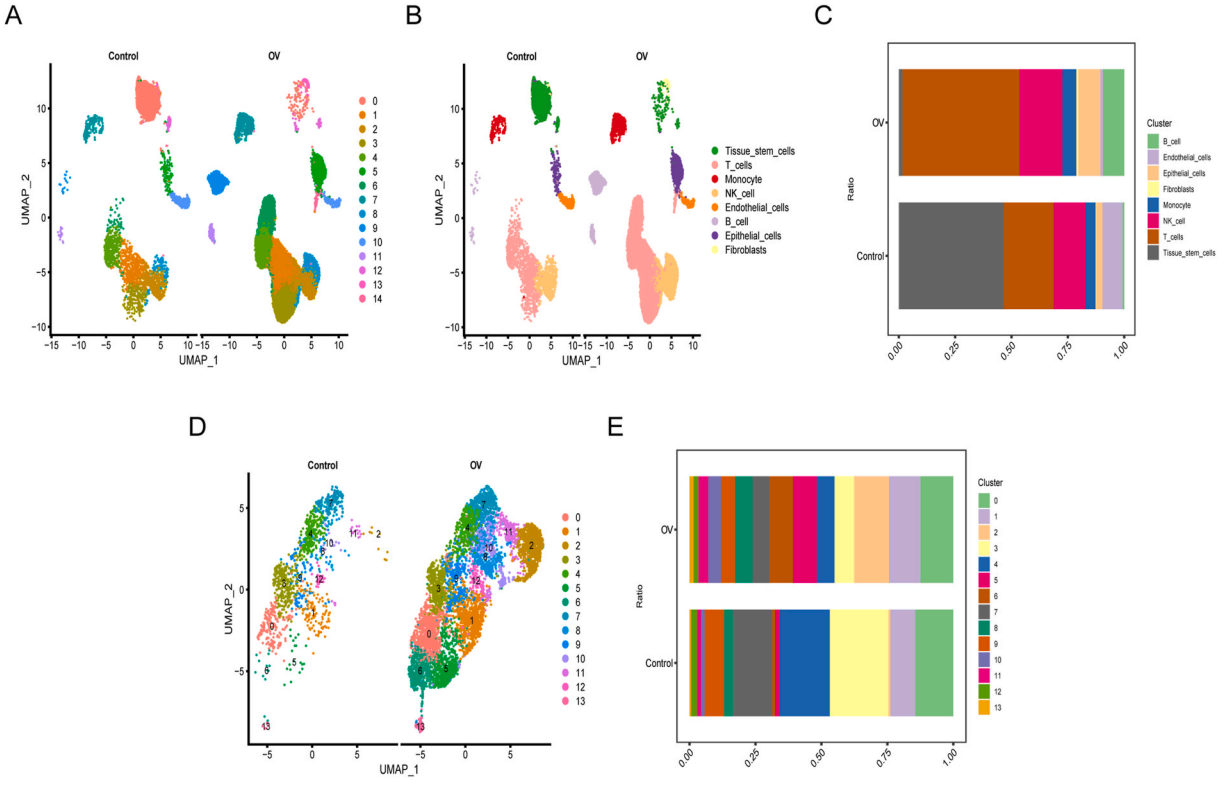

Fig. 1. Single cell analysis identified key T cell subsets. (A) Through UMAP analysis, a total of 15 cell clusters were identified in all samples. (B) 15 cell clusters are annotated as 8 highly heterogeneous cell types. (C) The proportion of 8 cell types between the OV sample group and the normal sample group. (D) The T cell subpopulations were subjected to another dimensionality reduction clustering analysis and displayed through the UMAP graph. (E) The proportion of T cell subpopulation related clusters between the OV sample group and the normal sample group.

free network of fibroblasts using a soft threshold of 7 to achieve optimal connectivity, researchers identified 8 distinct gene modules (Fig. 2A–D). A correlation analysis between the 8 gene modules and T cell subsets was performed, revealing significant correlations with clusters 2, 5, 6, 8, 10, and 11 (Fig. 2E and F). It is worth noting that cluster 2 shows a high correlation with turquoise and pink, cluster 5 shows a high correlation with yellow, red, and blue, cluster 6 shows a high correlation with turquoise, black, and red, cluster 8 shows a high correlation with turquoise, and cluster 10 shows a high correlation with green. As a result, the leading 100 genes from the turquoise, pink, yellow, red, blue, black, and green modules were chosen as hub genes for further analysis.

3.3. Functional annotation analysis and pseudo time analysis of hub genes

To investigate the biological mechanisms underlying hub genes, we performed GO and KEGG enrichment analyses on these genes. The findings from the GO analysis revealed a significant correlation of these hub genes with various biological processes including focal adhesion, cytochrome complexes, and respiratory chain complexes (Fig. 3A). Meanwhile, the KEGG analysis results indicated that the biological pathways like EB virus infection, cell apoptosis, human cytomegalovirus infection, and the NOD-like receptor signaling pathway are significantly associated with these hub genes (Fig. 3B).

To gain a deeper comprehension of T cell trajectories, a pseudo time analysis was performed. The differentiation of T cells revealed the presence of six unique states (Fig. 3C). Additionally, the magnitude of the blue hue corresponds to the duration of cell differentiation, where a darker shade of blue signifies the initiation of differentiation and a lighter shade indicates the migration of the most recently differentiated cells from right to left as time progresses (Fig. 3D). In Fig. 3E, the evolution and differentiation of cell subpopulations are depicted. Additionally, an examination was conducted on the alterations in gene expression of central genes during the differentiation of T cells. The heatmap in Fig. 3F illustrates the genes at the core that undergo changes during T cell differentiation. These findings indicate that hub genes could potentially serve varying functions in inducing the differentiation of T cells.

3.4. Construction and evaluation of a clinical prognosis model based on machine learning algorithms

Utilizing the hub genes mentioned above, we retrieved 301 DEGs from the TCGA-OV dataset. Subsequently, we performed univariate Cox analysis, resulting in the identification of 44 potential prognostic biomarkers (Fig. 4A and B). In Supplementary Table 1, we also show that these 44 differential prognostic genes correlate with the prognosis of OV patients. Through the application of the LOOCV framework on the TCGA-OV dataset, we tested 113 different predictive models and computed the C-index for each. An important observation was the RSF model, which exhibited the highest C-index of 0.748 (Fig. 4C). As a final step, a clinical prognostic model was developed using a selection of 10 T cell associated genes. Next, we investigated the copy number changes of these 10 T cells related genes. The CNV of ALOX5AP, LASP1, ISG20, and KRAS has significantly increased. The CNV of NBL1 has significantly

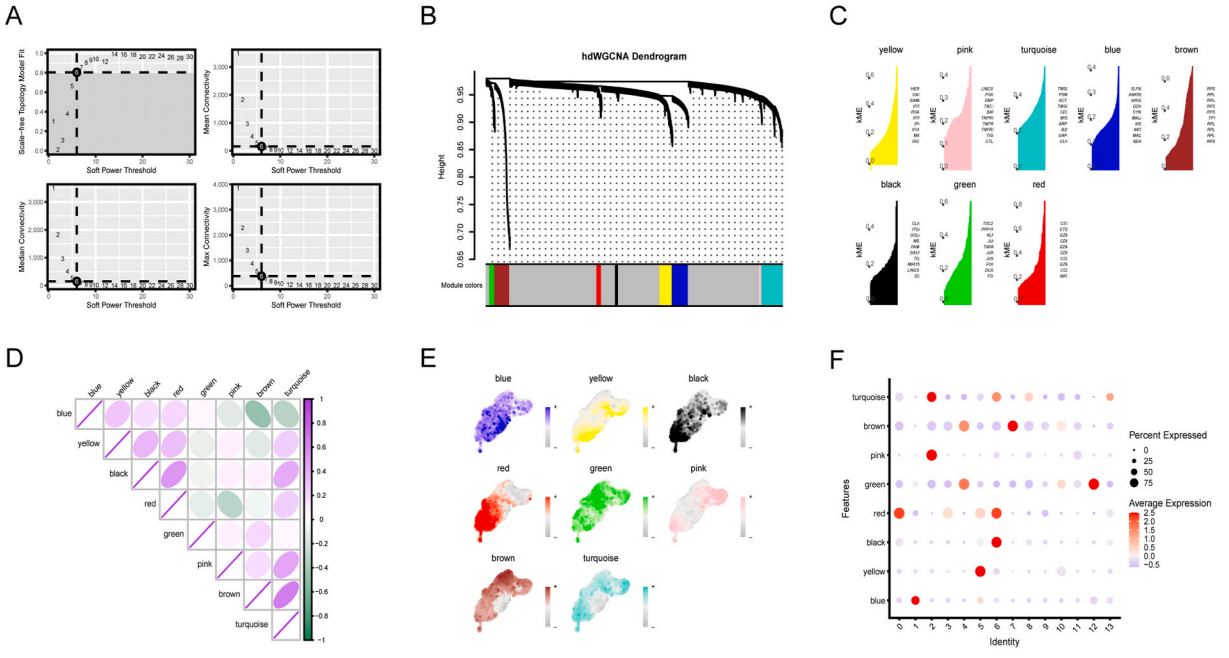

Fig. 2. HdWGCNA shows that turquoise, pink, yellow, red, blue, black, and green modules are seven central modules closely related to T cell subsets in OV. (A) Choose soft power = 6 to build a scale-free network. (B) Employ a tree diagram to depict the nine modules within a scale-free network. (C) Identified eight gene modules and showcased the principal genes via the hdWGCNA pipeline. (D) The eight gene modules' distribution across various T cell subpopulations. (E) Conduct correlation analysis among the different gene modules. (F) Explain the bubble diagram correlating the module with T cell subpopulations.

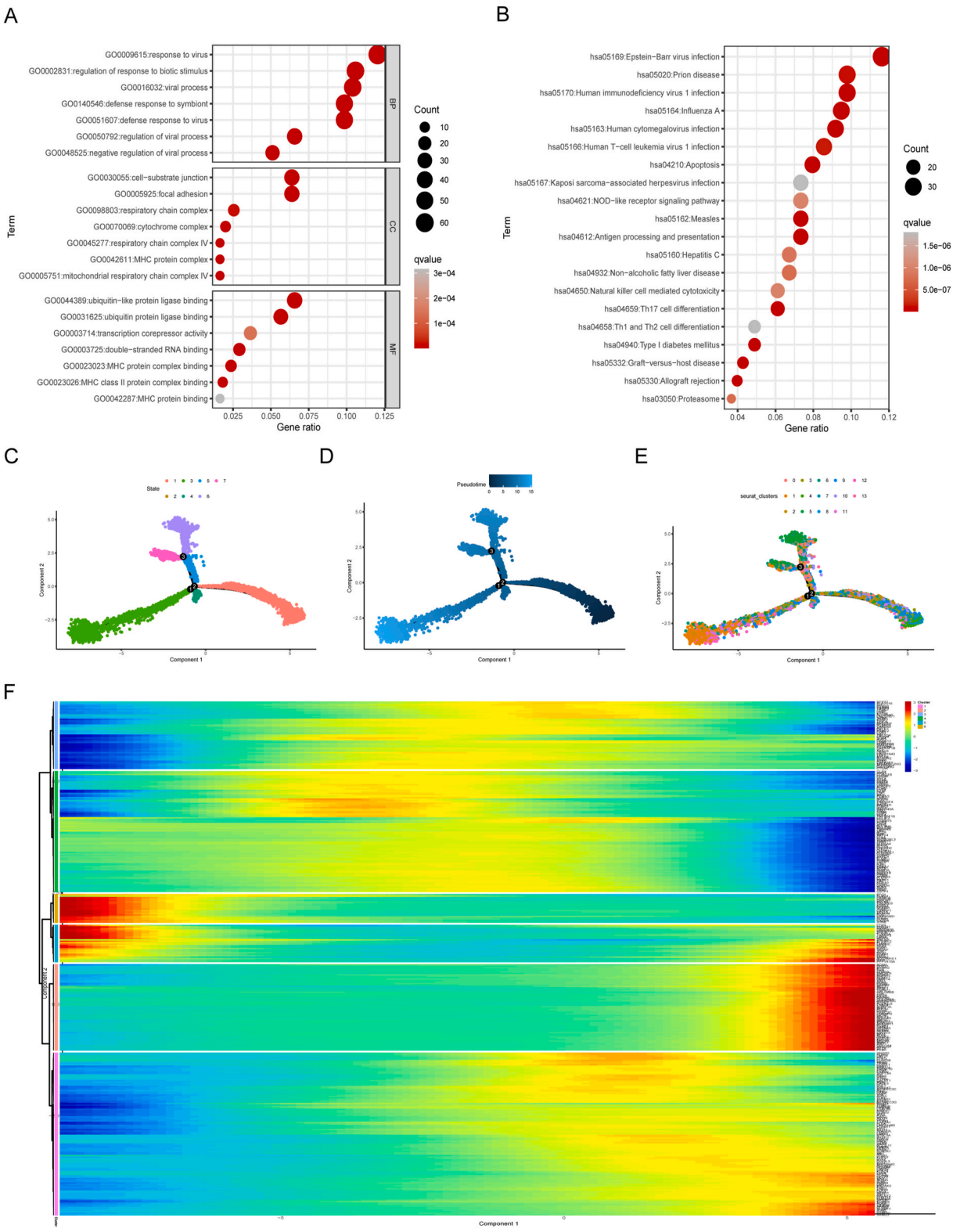

Fig. 3. Functional annotation analysis of hub genes. (A) Gene Ontology analysis of hub genes. (B) Kyoto Encyclopedia of Genes and Genomes analysis of hub genes. (C–E) Mapping a trajectory of differentiation based on cell differentiation status, coloring cell development time, and identifying cell clusters. (F) The expression heatmap of genes with simulated time values shows that genes with similar expression trends converge to form different clusters.

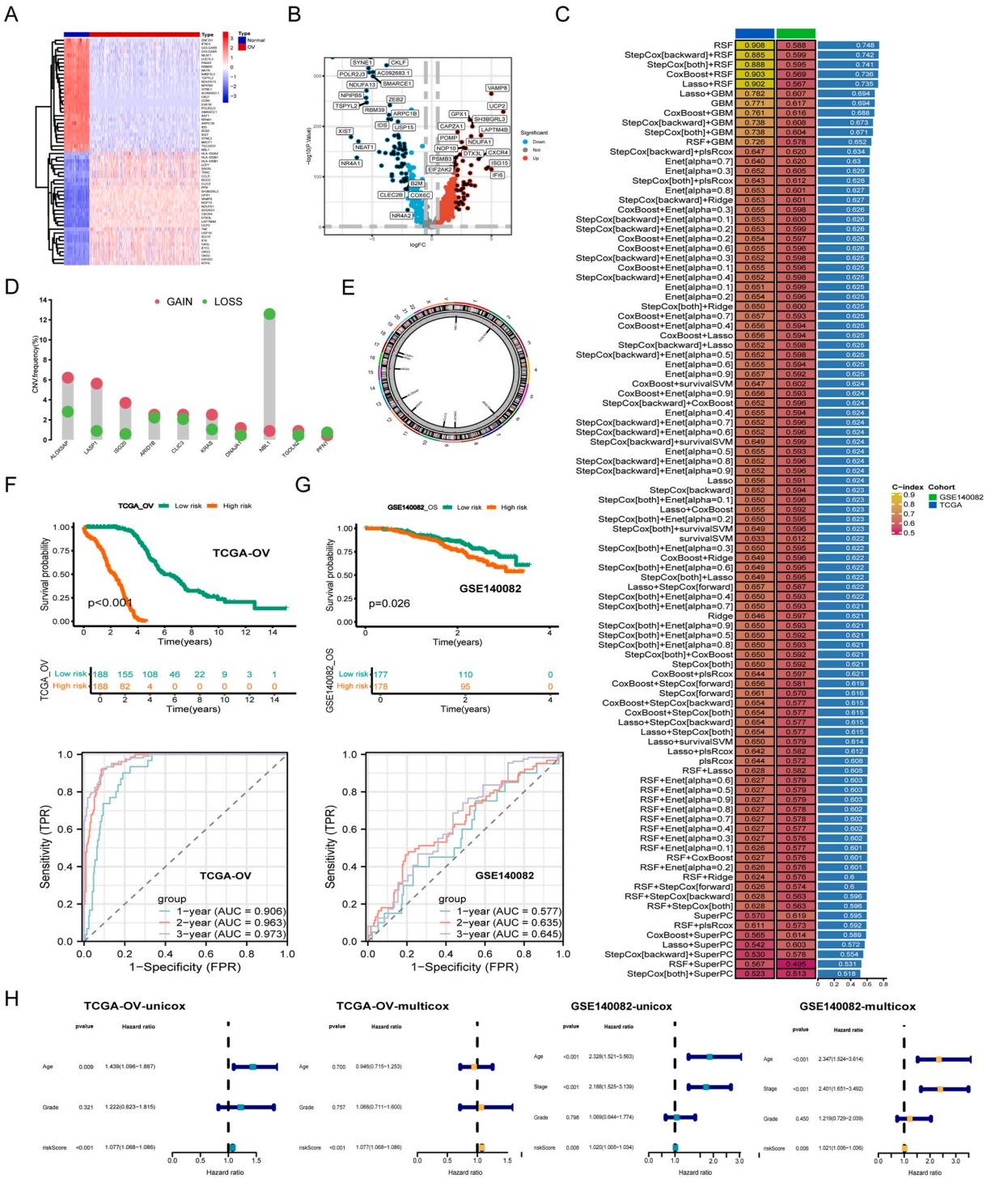

Fig. 4. Construct a clinical prognosis model and evaluate it using machine learning algorithms. (A, B) Differential expression analysis of hub genes between normal and OV samples. A: Heat map; B: Volcano map. (C) Calculate the C-index for each prognostic model created using 10 machine learning algorithms and 113 combinations in both the training and validation datasets. (D) Examine the frequency of copy number variations (CNVs) in 10 selected genes in TCGA-OV. Green indicates deletion frequency, while red dots represent amplification frequency. (E) Show the genomic locations of the 10 model genes on chromosomes. (F, G) Evaluate the survival and receiver operating characteristic (ROC) curves for OV patients classified into high-risk and low-risk groups in the training and validation datasets. F: TCGA-OV; G: GSE140082. (H) Perform univariate and multivariate Cox regression analyses considering clinical characteristics and risk scores of the clinical prognostic models in the training and validation datasets.

decreased (Fig. 4D). In Fig. 4E, each gene's chromosomal positions are presented, and the model's median risk score divides the TCGA-OV cohort (training set) and the GEO cohort (validation set) into high-risk and low-risk groups. In the TCGA-OV cohort, patients with low-risk OV exhibit a higher overall survival rate. ROC analysis was used to evaluate clinical prognostic models, yielding AUC values of 0.906, 0.963, and 0.973 for 1 year, 2 years, and 3 years, respectively (Fig. 4F). Similar to the results of the training set, low-risk OV patients in the GEO cohort also showed improved overall survival rates. The validity of the clinical prognostic model was confirmed using ROC analysis, where AUC values of 0.577, 0.635, and 0.645 were obtained for 1 year, 2 years, and 3 years, respectively (Fig. 4G). Furthermore, the risk score was validated as an independent predictor of clinical outcomes in OV patients in both the training and validation sets (Fig. 4H).

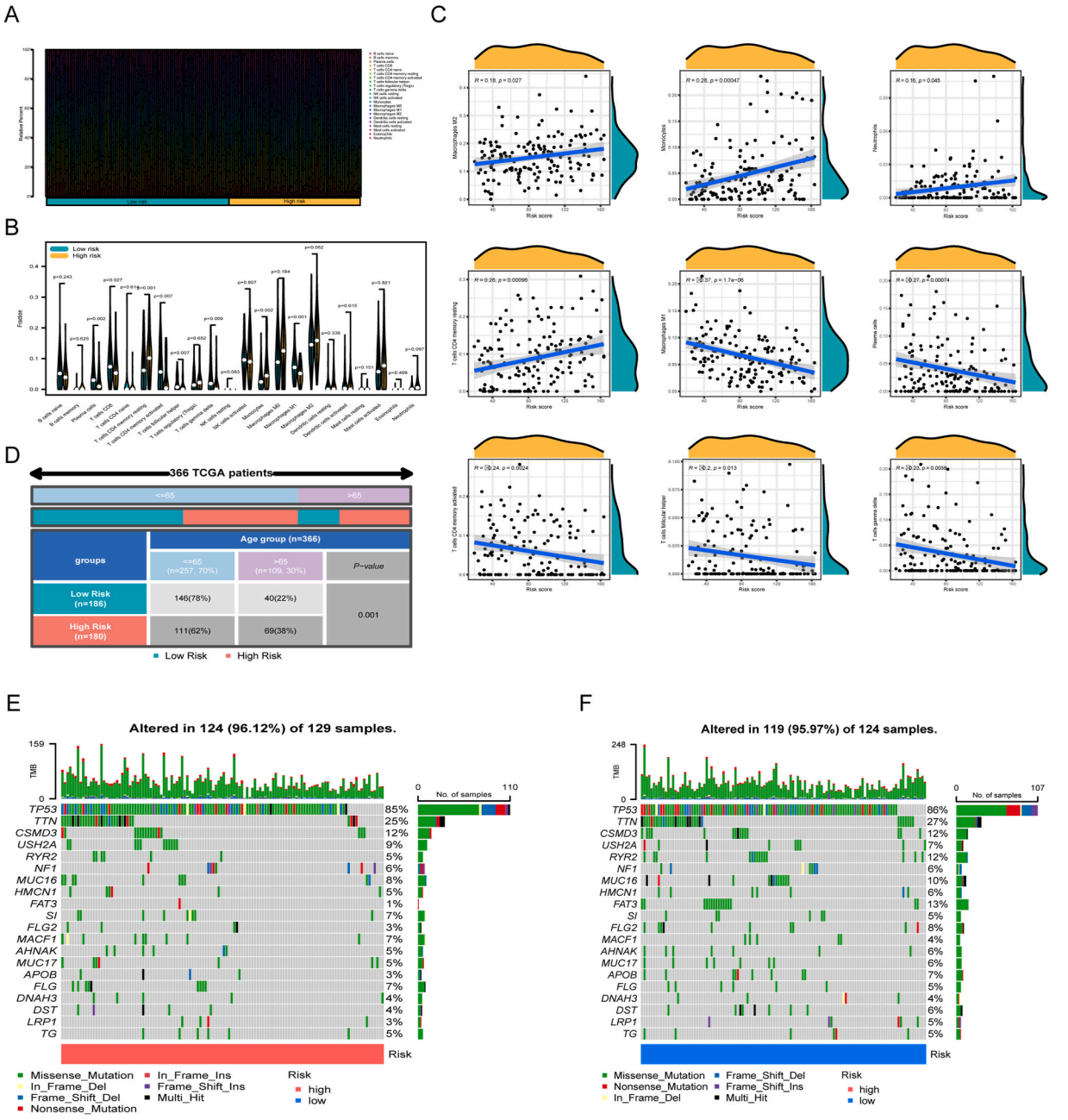

Fig. 5. Correlation between the risk score of clinical prognostic models and the TME of OV. (A) The proportion of immune cell infiltration is shown for each sample. (B) A comparison of immune cell infiltration levels is presented between high-risk and low-risk groups. (C) Displays the relationship between risk scores and immune cell presence. (D) Shows the correlation between risk scores and various clinical features. (E–F) Waterfall plots highlight somatic mutations in populations separated by risk level (E for high-risk; F for low-risk groups).

3.5. The correlation between the risk score of clinical prognostic models and the TME and TMB of OV

Fig. 5A delineates the infiltration ratio of immune cells across all samples for the high-risk and low-risk groups. There was a significant relationship identified between resting memory CD4 T cells and monocytes within the high-risk category. Conversely, the low-risk category displayed significant associations among plasma cells, CD8 T cells, activated memory CD4 T cells, follicular helper T cells, gamma delta T cells, and M1 Macrophages, as shown in Fig. 5B. Additionally, Macrophages M2, monocytes, neutrophils, and resting memory CD4 T cells displayed positive correlations with risk scores, whereas M1 Macrophages, plasma cells, activated memory CD4 T cells, follicular helper T cells, and gamma delta T cells showed negative correlations with risk scores, as demonstrated in Fig. 5C. Furthermore, a noteworthy relationship was detected between risk score and patient age, as depicted in Fig. 5D. The mutation frequency of the top 20 genes for both high-risk and low-risk groups is presented in the waterfall plots in Fig. 5E and F.

3.6. Drug sensitivity analysis of different risk groups

Chemotherapy plays a crucial role in the treatment of ovarian cancer alongside surgery. Our research involved examining the potency of commonly used drugs by measuring their IC50 values in both high-risk and low-risk patient groups. A comparative study revealed that AZD1332, BMS-536924, BMS-754807, ERK-2440, Foretinib, NVP-ADW742, and Taselisib had significantly higher IC50 levels in low-risk patients than in high-risk patients, suggesting their potential efficacy for the former (Fig. 6A–G). Conversely, the IC50 value of ML323 was lower in the low-risk group compared to the high-risk group, indicating its possible effectiveness in treating high-risk patients (Fig. 6H).

3.7. PFN1 is upregulated in human OV cell lines

We initially tested the markers identified by the predictive model in the human normal ovarian cell line IOSE80, alongside the OV cell lines A2780 and HEY. Transcription of A2780 and HEY differed from that of IOSE80. Among the 10 markers, PFN1 was significantly up-regulated in OV cell lines, while the other markers were not as significant. For this reason, we chose PFN1 for subsequent validation (Figs. 7 and 8).

3.8. PFN1 promotes the progression of OV in vitro

We first validated the inhibitory efficiency of small interfering RNAs for PFN1 in A2780 versus HEY cell lines. Both of two small interfering RNAs against different targets showed good efficiency (Fig. 9A and C). The results of CCK8 suggested that cell viability was significantly suppressed upon inhibition of PFN1 expression in A2789 and HEY (Fig. 9B and D). Furthermore, the inhibiting of PFN1 also resulted in a significant reduction in the proliferative ability of the cells (Fig. 9E–G). The cellular senescence marker, P21, was re-upregulated after PFN1 inhibition. Recovery of P21 was also accompanied by recovery of apoptotic maker, BAX. Epithelial

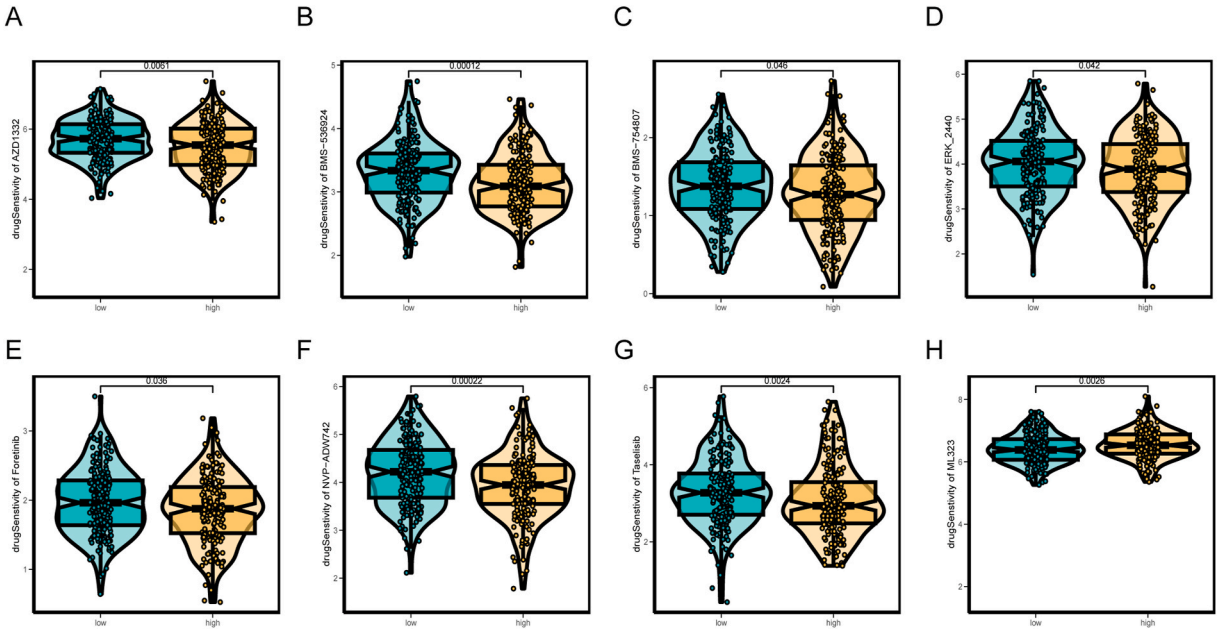

Fig. 6. Drug sensitivity analysis of high-risk and low-risk populations. (A) AZD1332. (B) BMS -536924. (C) BMS -754807. (D) ERK_2440. (E) Foretinib. (F) NVP-ADW742. (G) Taselisib. (H)ML323.

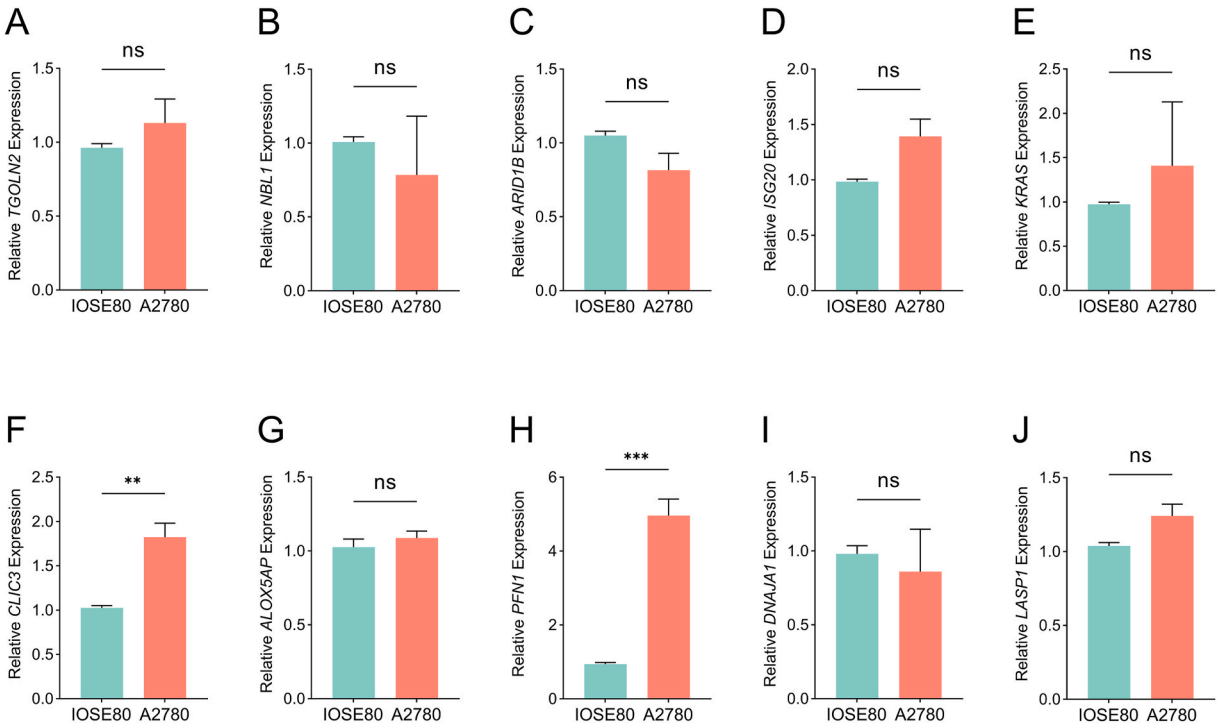

Fig. 7. PFN1 is upregulated in human OV cell line A2780. (A–J) PCR was conducted to assess the transcript levels of TGOLN2, NBL1, ARID1B, ISG20, KRAS, CLIC3, ALOX5AP, PFN1, DNAJA1, and LASP1 in human normal ovarian epithelial cells (IOSE80) and the human OV cell line A2780. N = 3/group. ***≤0.001.

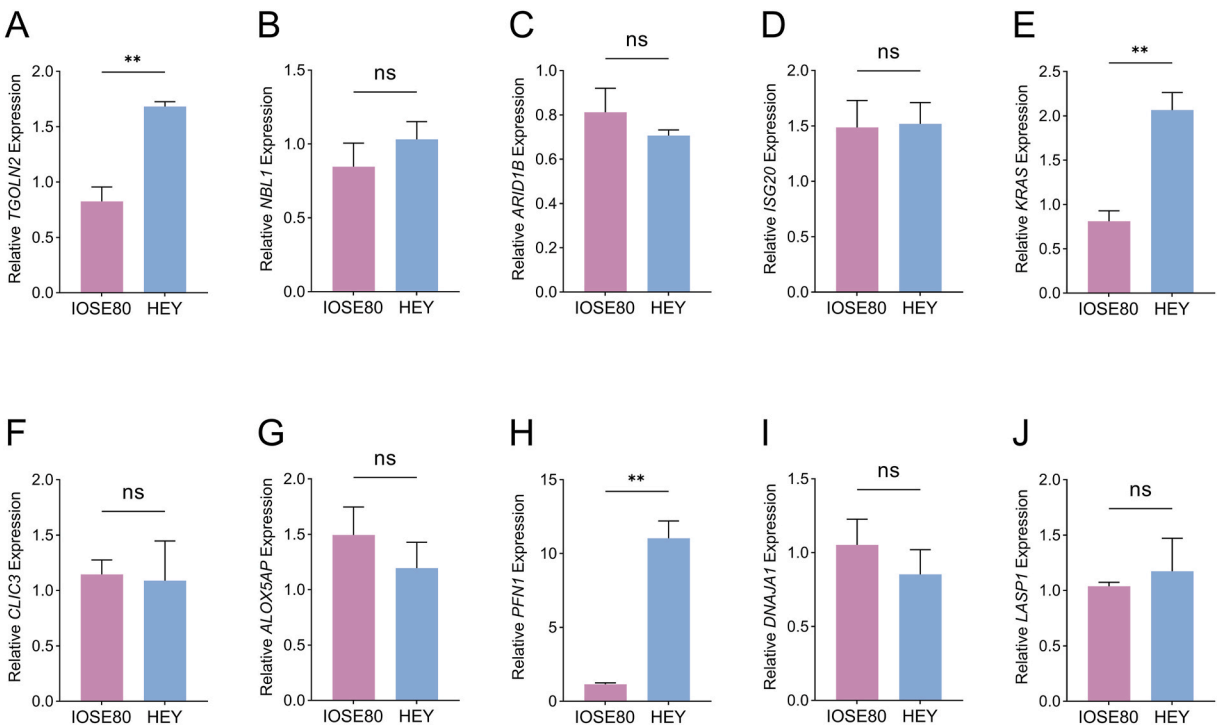

Fig. 8. PFN1 is upregulated in human OV cell line HEY. (A–J) PCR was performed to detect the transcript levels of TGOLN2, NBL1, ARID1B, ISG20, KRAS, CLIC3, ALOX5AP, PFN1, DNAJA1, and LASP1 in human normal ovarian epithelial cells, IOSE80, and in human OV cell line, HEY. N = 3/group. **≤0.01.

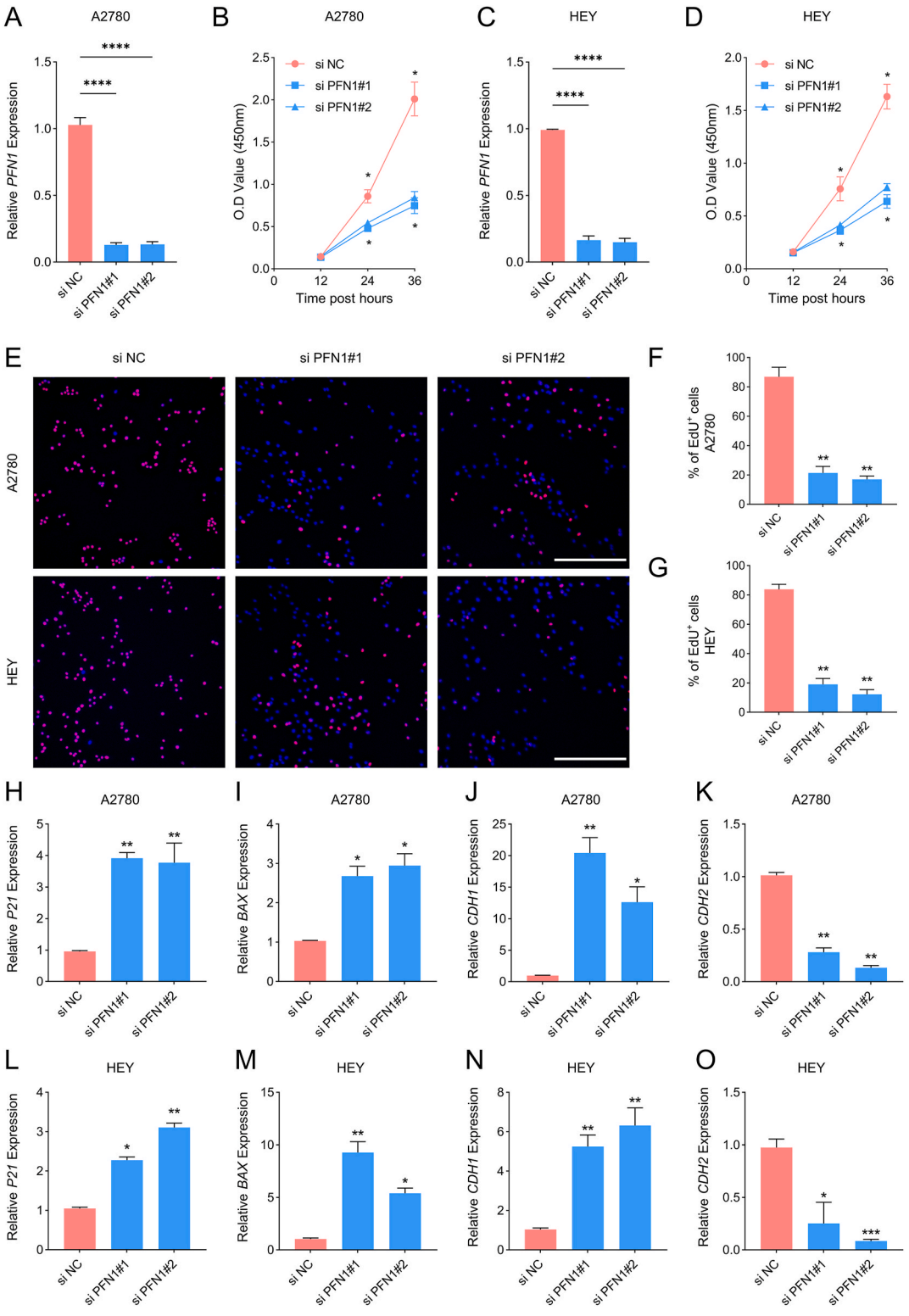

(caption on next page)

Fig. 9. PFN1 promotes the progression of OV in vitro. (A) Detection of the efficiency of PFN1 expression inhibited by small interfering RNA in the A2780 cell line. (B) Changes in cell line viability of A2780 cells after inhibition of PFN1. (C) Detection of the efficiency of PFN1 expression inhibited by small interfering RNA in the HEY cell line. (D) Changes in cell line viability of HEY cells after inhibition of PFN1. (E–G) Alterations in the proliferative capacity of A2780 and HEY cell lines after inhibition of PFN1. (H–K) Alterations in the transcription of P21, BAX, CDH1 and CDH2 following inhibition of PFN1 in the A2780 cell line. (L–O) Alterations in the transcription of P21, BAX, CDH1 and CDH2 following inhibition of PFN1 in the HEY cell line. N = 3. *≤0.05, **≤0.01, ***≤0.001, ****≤0.0001. The results are presented as mean ± SD.

mesenchymal transition (EMT) of cells was similarly altered upon PFN1 inhibition, as evidenced by restoration of CDH1 as well as inhibition of CDH2 (Fig. 9H–O).

4. Discussion

OV is a leading factor in female cancer mortality, with its aggressive nature and vague initial signs leading to late-stage detection in the majority of cases [30]. Although surgery and chemotherapy are currently the standard treatment methods, the drug resistance and immune suppression in OV patients still lead to unsatisfactory survival rates [31]. In recent years, immunotherapy, especially research on T cells, has provided new hope for the treatment of OV. cells are crucial effector cells against tumors in TME, exhibiting cytotoxic properties and serving a critical function in eliminating cancer cells [32]. Thus, a comprehensive examination of the underlying mechanisms concerning T cells in OV can unveil pivotal immune evasion pathways and novel therapeutic targets. This can offer substantial theoretical backing for tailoring personalized treatment approaches for individuals with OV.

In this study, we identified T cell subsets as characteristic cell subsets of OV by analyzing OV single-cell data. Subsequently, using the hdWGCNA method, the gene modules related to T cell subsets were elucidated, which helps to identify the key genes involved in OV development. Functional annotation analysis highlights their involvement in key biological processes, including EB virus infection, cell apoptosis, human cytomegalovirus infection, and NOD like receptor signaling pathways. Apoptosis is a programmed cell death mechanism aimed at maintaining cellular balance and clearing abnormal cells in the body [33]. Cell apoptosis is mainly triggered by different cellular stressors, like DNA damage, cellular aging, or external signals [34]. Evading apoptosis is a critical feature of cancer, as cancer cells can create ways to escape apoptosis and boost their survival, growth, and resistance to therapy [35]. In TME, apoptosis serves as a protective barrier against the proliferation of cancer cells [36]. The dysregulation of multiple apoptotic signaling pathways, including endogenous mitochondrial pathways and exogenous death receptor pathways, in cancer has been widely reported [37]. The family of genes known as Bcl-2, which consists of Bcl-2, Bcl-xL, and Bax, plays a crucial role in regulating cell apoptosis [38,39]. The proteins Bcl-2 and Bcl-xL, with their anti-apoptotic properties, have the ability to inhibit signals that lead to cell death, and are frequently linked to unfavorable cancer outcomes. On the other hand, Bax, a pro-apoptotic protein, enhances the process of cell apoptosis [40]. When the members of the Bcl-2 gene family are not properly regulated, it can hinder cell apoptosis and elevate the survival rate of tumor cells. In OV, tumor cells can utilize various mechanisms to avoid apoptosis, thereby achieving uncontrolled proliferation advantages [41]. The study by Sijia Ma et al. found that TGFBI can be upregulated by HIF-2 α and promote OV chemotherapy resistance by interfering with cell apoptosis and activating the PI3K/Akt pathway to promote DNA damage repair [42]. In summary, in-depth research on the mechanism of cell apoptosis in OV can help understand the occurrence and development of tumors.

Based on these hub genes, we conducted univariate Cox analysis to determine potential prognostic biomarkers for OV. Afterwards, we used the LOOCV framework to fit 113 types of predictive models and developed accurate and stable clinical prognostic models containing ten genes (TGOLN2, NBL1, ARID1B, ISG20, KRAS, CLIC3, ALOX5AP, PFN1, DNAJA1, and LASP1). The findings show that the best model is the RSF model, which boasts an impressive average C-index of 0.748. This particular model excels in accurately categorizing patients. The risk score calculated within this clinical prognostic model was found to be a significant and independent risk factor for predicting clinical outcomes in ovarian cancer patients, according to both univariate and multivariate COX analyses conducted in the training and validation sets. ROC analysis has demonstrated that the model has excellent clinical value. Following this, we carried out experimental validation on the ten genes used to build the model. The results indicated a significant upregulation of PFN1 in OV cell lines. The results of CCK8 indicate that after PFN1 expression is inhibited, cell viability is significantly inhibited and cell proliferation ability is significantly reduced. The cell aging marker P21 was re upregulated after PFN1 inhibition. The recovery of P21 is also accompanied by the recovery of apoptosis marker BAX. Furthermore, after PFN1 inhibition, similar changes occurred in the epithelial mesenchymal transition of cells. Profilin 1 (PFN1) belongs to the actin-binding protein family and plays specific roles in cell migration and malignant tumors [43,44]. A study carried out by Jing Zhang and co-authors revealed that HLA-F-AS1 boosts PFN1 expression in extracellular vesicles of colorectal cancer (CRC) through miR-375 inhibition. This process drives macrophage polarization towards the M2 phenotype, thereby aiding in CRC advancement [45]. Another study led by Ni Bai and team revealed that suppressing lncRNA HCP5 can impede the advancement of colorectal cancer by modulating the miR-299-3p/PFN1/AKT pathway [46]. AKT serves as a crucial actor in various cancer types [47]. Additionally, PFN1 has the ability to initiate AKT signaling in breast cancer and regulate the integrin/focal adhesion kinase pathway in gastric cancer [48,49]. The report by David M Gau et al. on suggests that high expression of PFN1 is related with OV associated with BRCA1 deficiency [50]. Therefore, we hypothesize that inhibiting PFN1 can regulate the recovery of P21 and promote the recovery of apoptosis marker BAX, thereby promoting cell apoptosis and inhibiting the development of OV.

The presence of an immunosuppressive setting plays a crucial role in the unfavorable outcomes seen in OV patients. Our research uncovered significant discrepancies in the infiltration of immune cells across various risk groups. We identified substantial disparities

in the levels of diverse immune cell subcategories infiltrating tumors in high-risk versus low-risk cohorts. Notably, the high-risk category exhibited a strong correlation between CD4 T cell memory resting and monocytes, while the low-risk group displayed significant associations with plasma cells, CD8 T cells, CD4 T cells memory activated, T cells follicular helper, T cells gamma delta, and M1 macrophages. These findings imply that distinct populations of immune cells might exert varying effects on the prognosis of OV patients. Eiichi Sato et al. reported that CD8+T cells can eradicate OV cells and are associated with good patient survival [17]. We believe that this may be one of the reasons why low-risk patients have survival advantages. Additional correlation analysis reveals a positive correlation between the risk score and M2 macrophages, monocytes, neutrophils, as well as CD4 T cells memory at rest. These specific cell types dominate in patients at a heightened risk and could be linked to the invasiveness and advancement of tumors. Conversely, M1 macrophages, plasma cells, CD4 T cells memory activated, T cells follicular helper, and T cells gamma delta display an inverse relationship with risk scores, indicating that these immune cells are more prevalent in the group with a lower risk and may generate anti-tumor responses, hindering tumor proliferation and dissemination. In inflammation research, M1 macrophages are generally considered to have a promoting effect on inflammation, while M2 macrophages are generally considered to have an inhibitory effect on inflammation. Contrary to the study of inflammation, M2 macrophages possess the ability to suppress inflammation and stimulate tumor growth within the tumor associated macrophages. There exist four distinguishable varieties of M2 macrophages: M2a, M2b, M2c, and M2d. M2a macrophages boost the endocytosis process, M2b macrophages have the ability to generate both inflammatory and anti-inflammatory cytokines, M2c macrophages are experts in phagocytosing apoptotic cells, and M2d macrophages play a role in angiogenesis and tumor advancement [51–53]. Bo Sheng et al. found that CPNE1 can promote M2 macrophage activation, leading to accelerated development of OV [54]. These findings contribute to our comprehension of the immune microenvironment in OV, underscoring the vital functions of T cells and macrophages in tumor immune evasion as well as anti-tumor immune reactions [55]. The results propose that altering the immune microenvironment could be a hopeful strategy to enhance the results of high-risk patients with ovarian cancer. Moreover, resistance to chemotherapy continues to be a notable element influencing the grim prognosis in individuals with ovarian cancer [56]. In this study, we created a prognostic model aimed at efficiently categorizing patients into high-risk and low-risk groups. The analysis of drug responses indicated that those classified under the low-risk group displayed better responses to chemotherapy drugs. The prognostic model's utility extends to predicting immunotherapy and chemotherapy outcomes for individuals with OV. These findings offer novel perspectives and pathways for advancing targeted immunotherapy moving forward.

The limitations in our research persist. Initially, a majority of the analysis conducted in this study relied on information sourced from public databases. Consequently, additional confirmation is required for the clinical prognostic model developed in this research, particularly through larger sample size cohorts and additional clinical data. It is essential to perform further in vitro and in vivo studies to explore and validate the mechanism of action of the potential biomarker PFN1 in ovarian cancer.

5. Conclusion

A precise and consistent clinical prognostic model has been developed for OV, effectively predicting clinical outcomes and accurately categorizing patients. This enables accurate prediction of responses to immune therapy and chemotherapy. This study improves our comprehension of the immune environment in OV and offers novel perspectives for crafting directed immunotherapies and personalized treatment strategies. Altering the immune environment and focusing on the pivotal gene PFN1 hold potential for enhancing the outlook of high-risk OV individuals and boosting treatment efficiency.

Data availability statement

All public data comes from the TCGA database (https://portal.gdc.cancer.gov) and GEO database (https://www.ncbi.nlm.nih.gov/geo/).

Ethics statement

None.

Conflict of interest

The authors report no conflicts of interest in this work.

Funding

This research was supported by the Scientific Research Project of the Nantong Municipal Health Commission (Grant No. MS2023017), This research was supported by the Research Hospital Construction Fund and the "Leading Talent in Scientific Research" Development Fund for Research Physicians at the Affiliated Hospital of Nantong University (Grant No. YJXYY202204-YS1303), National Key Research and Development Program of China (Grant No. 2022YFC2702500), National Natural Science Foundation of China (Grant No. 82371659), the Research Foundation of Guangzhou Women and Children's Medical Center for Clinical Doctor (2023BS024), the Science and Technology Program of Guangzhou, China (2024A03J1087, 2024A04J4164).

CRediT authorship contribution statement

Qiwang Lin: Writing – original draft, Conceptualization. **Weixu Ma:** Writing – original draft, Conceptualization. **Mengchang Xu:** Formal analysis, Data curation. **Zijin Xu:** Formal analysis, Data curation. **Jing Wang:** Formal analysis, Data curation. **Zhu Liang:** Formal analysis, Data curation. **Lin Zhu:** Validation. **Menglu Wu:** Validation. **Jiejun Luo:** Validation. **Haiying Liu:** Writing – review & editing, Conceptualization. **Jianqiao Liu:** Writing – review & editing, Conceptualization. **Yunfeng Jin:** Writing – review & editing, Conceptualization.

Declaration of competing interest

The authors declare that they have no known competing financial interests or personal relationships that could have appeared to influence the work reported in this paper.

Acknowledgment

None.

Appendix A. Supplementary data

Supplementary data to this article can be found online at https://doi.org/10.1016/j.heliyon.2024.e36898.

References

[1] P.A. Konstantinopoulos, U.A. Matulonis, Clinical and translational advances in ovarian cancer therapy, Nature cancer 4 (9) (2023) 1239–1257.
[2] I.J. Jacobs, U. Menon, A. Ryan, et al., Ovarian cancer screening and mortality in the UK Collaborative Trial of Ovarian Cancer Screening (UKCTOCS): a randomised controlled trial, Lancet (London, England) 387 (10022) (2016) 945–956.
[3] M.H. Ebell, M.B. Culp, T.J. Radke, A systematic review of symptoms for the diagnosis of ovarian cancer, Am. J. Prev. Med. 50 (3) (2016) 384–394.
[4] F. Bray, J. Ferlay, I. Soerjomataram, R.L. Siegel, L.A. Torre, A. Jemal, Global cancer statistics 2018: GLOBOCAN estimates of incidence and mortality worldwide for 36 cancers in 185 countries, CA A Cancer J. Clin. 68 (6) (2018) 394–424.
[5] Y. Guo, S. Li, C. Li, L. Wang, W. Ning, Multifactor assessment of ovarian cancer reveals immunologically interpretable molecular subtypes with distinct prognoses, Front. Immunol. 14 (2023) 1326018.
[6] S. Bose, P. Saha, B. Chatterjee, A.K. Srivastava, Chemokines driven ovarian cancer progression, metastasis and chemoresistance: potential pharmacological targets for cancer therapy, Semin. Cancer Biol. 86 (Pt 2) (2022) 568–579.
[7] O. Kopper, C.J. de Witte, K. Lõhmussaar, et al., An organoid platform for ovarian cancer captures intra- and interpatient heterogeneity, Nat. Med. 25 (5) (2019) 838–849.
[8] D.C. Hinshaw, L.A. Shevde, The tumor microenvironment innately modulates cancer progression, Cancer Res. 79 (18) (2019) 4557–4566.
[9] Y. Dai, W. Qiang, K. Lin, Y. Gui, X. Lan, D. Wang, An immune-related gene signature for predicting survival and immunotherapy efficacy in hepatocellular carcinoma, Cancer Immunol. Immunother. : CII. 70 (4) (2021) 967–979.
[10] S.H. Kiaie, H. Salehi-Shadkami, M.J. Sanaei, et al., Nano-immunotherapy: overcoming delivery challenge of immune checkpoint therapy, J. Nanobiotechnol. 21 (1) (2023) 339.
[11] R. Su, J. Gu, J. Sun, et al., CaCO(3) powder-mediated biomineralization of antigen nanosponges synergize with PD-1 blockade to potentiate anti-tumor immunity, J. Nanobiotechnol. 21 (1) (2023) 120.
[12] K. Pang, Z.D. Shi, L.Y. Wei, et al., Research progress of therapeutic effects and drug resistance of immunotherapy based on PD-1/PD-L1 blockade, Drug Resist. Updates : reviews and commentaries in antimicrobial and anticancer chemotherapy 66 (2023) 100907.
[13] M. Melssen, C.L. Slingluff Jr., Vaccines targeting helper T cells for cancer immunotherapy, Curr. Opin. Immunol. 47 (2017) 85–92.
[14] R. Kennedy, E. Celis, Multiple roles for CD4+ T cells in anti-tumor immune responses, Immunol. Rev. 222 (2008) 129–144.
[15] H. Dong, C. Xie, Z. Yao, et al., PTPRO-related CD8(+) T-cell signatures predict prognosis and immunotherapy response in patients with breast cancer, Front. Immunol. 13 (2022) 947841.
[16] M. Zhang, J. Ma, Q. Guo, S. Ding, Y. Wang, H. Pu, CD8(+) T cell-associated gene signature correlates with prognosis risk and immunotherapy response in patients with lung adenocarcinoma, Front. Immunol. 13 (2022) 806877.
[17] E. Sato, S.H. Olson, J. Ahn, et al., Intraepithelial CD8+ tumor-infiltrating lymphocytes and a high CD8+/regulatory T cell ratio are associated with favorable prognosis in ovarian cancer, Proc. Natl. Acad. Sci. U.S.A. 102 (51) (2005) 18538–18543.
[18] M.H. Shahrajabian, W.L. Sun, Survey on multi-omics, and multi-omics data analysis, integration and application, Curr. Pharmaceut. Anal. 19 (4) (2023) 267–281.
[19] H. Zhang, T. Liu, Z. Zhang, et al., Integrated proteogenomic characterization of human high-grade serous ovarian cancer, Cell 166 (3) (2016) 755–765.
[20] B. Ding, Z. Ye, H. Yin, et al., Comprehensive single-cell analysis reveals heterogeneity of fibroblast subpopulations in ovarian cancer tissue microenvironment, Heliyon 10 (6) (2024) e27873.
[21] H. Zhao, Y. Teng, W. Hao, et al., Single-cell analysis revealed that IL4I1 promoted ovarian cancer progression, J. Transl. Med. 19 (1) (2021) 454.
[22] J.T. Leek, W.E. Johnson, H.S. Parker, A.E. Jaffe, J.D. Storey, The sva package for removing batch effects and other unwanted variation in high-throughput experiments, Bioinformatics 28 (6) (2012) 882–883.
[23] J.T. Leek, R.B. Scharpf, H.C. Bravo, et al., Tackling the widespread and critical impact of batch effects in high-throughput data, Nat. Rev. Genet. 11 (10) (2010) 733–739.
[24] T. Stuart, A. Butler, P. Hoffman, et al., Comprehensive integration of single-cell data, Cell 177 (7) (2019) 1888–1902.e1821.
[25] Z.C. Lu, Z.H. Wang, Z.H. Song, et al., Single-cell sequencing of brain tissues reveal the central nervous system's susceptibility to SARS-CoV-2 and the drug, Front. Pharmacol. 13 (2022).
[26] S. Morabito, F. Reese, N. Rahimzadeh, E. Miyoshi, V. Swarup, hdWGCNA identifies co-expression networks in high-dimensional transcriptomics data, Cell reports methods 3 (6) (2023) 100498.
[27] A. Mayakonda, D.C. Lin, Y. Assenov, C. Plass, H.P. Koeffler, Maftools: efficient and comprehensive analysis of somatic variants in cancer, Genome Res. 28 (11) (2018) 1747–1756.

[28] P. Geeleher, N.J. Cox, R.S. Huang, Clinical drug response can be predicted using baseline gene expression levels and in vitro drug sensitivity in cell lines, Genome Biol. 15 (3) (2014) R47.
[29] P. Geeleher, N. Cox, R.S. Huang, pRRophetic: an R package for prediction of clinical chemotherapeutic response from tumor gene expression levels, PLoS One 9 (9) (2014) e107468.
[30] A. Raza, A. Singh, S. Amin, J.E. Spallholz, A.K. Sharma, Identification and biotin receptor-mediated activity of a novel seleno-biotin compound that inhibits viability of and induces apoptosis in ovarian cancer cells, Chem. Biol. Interact. 365 (2022) 110071.
[31] V. Gogineni, S. Morand, H. Staats, et al., Current ovarian cancer maintenance strategies and promising new developments, J. Cancer 12 (1) (2021) 38–53.
[32] S. Jhunjhunwala, C. Hammer, L. Delamarre, Antigen presentation in cancer: insights into tumour immunogenicity and immune evasion, Nat. Rev. Cancer 21 (5) (2021) 298–312.
[33] S. Elmore, Apoptosis: a review of programmed cell death, Toxicol. Pathol. 35 (4) (2007) 495–516.
[34] A. Ashkenazi, G. Salvesen, Regulated cell death: signaling and mechanisms, Annu. Rev. Cell Dev. Biol. 30 (2014) 337–356.
[35] X. Jing, F. Yang, C. Shao, et al., Role of hypoxia in cancer therapy by regulating the tumor microenvironment, Mol. Cancer 18 (1) (2019) 157.
[36] K. Yaacoub, R. Pedeux, K. Tarte, T. Guillaudeux, Role of the tumor microenvironment in regulating apoptosis and cancer progression, Cancer Lett. 378 (2) (2016) 150–159.
[37] A. Strasser, S. Cory, J.M. Adams, Deciphering the rules of programmed cell death to improve therapy of cancer and other diseases, EMBO J. 30 (18) (2011) 3667–3683.
[38] Y. Yu, B. Liu, X. Li, et al., ATF4/CEMIP/PKCα promotes anoikis resistance by enhancing protective autophagy in prostate cancer cells, Cell Death Dis. 13 (1) (2022) 46.
[39] H.D. Xu, Z.H. Qin, Beclin 1, bcl-2 and autophagy, Adv. Exp. Med. Biol. 1206 (2019) 109–126.
[40] N. Popgeorgiev, J.D. Sa, L. Jabbour, et al., Ancient and conserved functional interplay between Bcl-2 family proteins in the mitochondrial pathway of apoptosis, Sci. Adv. 6 (40) (2020).
[41] S. Fulda, K.M. Debatin, Extrinsic versus intrinsic apoptosis pathways in anticancer chemotherapy, Oncogene 25 (34) (2006) 4798–4811.
[42] H. Mai, X. Yang, Y. Xie, et al., Identification of the shared hub gene signatures and molecular mechanisms between HIV-1 and pulmonary arterial hypertension, Sci. Rep. 14 (1) (2024) 7048.
[43] J.R. Karamchandani, M.Y. Gabril, R. Ibrahim, et al., Profilin-1 expression is associated with high grade and stage and decreased disease-free survival in renal cell carcinoma, Hum. Pathol. 46 (5) (2015) 673–680.
[44] G. Mouneimne, S.D. Hansen, L.M. Selfors, et al., Differential remodeling of actin cytoskeleton architecture by profilin isoforms leads to distinct effects on cell migration and invasion, Cancer Cell 22 (5) (2012) 615–630.
[45] J. Zhang, S. Li, X. Zhang, C. Li, J. Zhang, W. Zhou, LncRNA HLA-F-AS1 promotes colorectal cancer metastasis by inducing PFN1 in colorectal cancer-derived extracellular vesicles and mediating macrophage polarization, Cancer Gene Ther. 28 (12) (2021) 1269–1284.
[46] N. Bai, Y. Ma, J. Zhao, B. Li, Knockdown of lncRNA HCP5 suppresses the progression of colorectal cancer by miR-299-3p/PFN1/AKT Axis, Cancer Manag. Res. 12 (2020) 4747–4758.
[47] M. Kono, T. Fujii, B. Lim, M.S. Karuturi, D. Tripathy, N.T. Ueno, Androgen receptor function and androgen receptor-targeted therapies in breast cancer: a review, JAMA Oncol. 3 (9) (2017) 1266–1273.
[48] T. Das, Y.H. Bae, A. Wells, P. Roy, Profilin-1 overexpression upregulates PTEN and suppresses AKT activation in breast cancer cells, J. Cell. Physiol. 218 (2) (2009) 436–443.
[49] Y.J. Cheng, Z.X. Zhu, J.S. Zhou, et al., Silencing profilin-1 inhibits gastric cancer progression via integrin β1/focal adhesion kinase pathway modulation, World J. Gastroenterol. 21 (8) (2015) 2323–2335.
[50] D.M. Gau, J.L. Lesnock, B.L. Hood, et al., BRCA1 deficiency in ovarian cancer is associated with alteration in expression of several key regulators of cell motility - a proteomics study, Cell Cycle 14 (12) (2015) 1884–1892.
[51] S. Yang, J. Du, W. Wang, D. Zhou, X. Xi, APOC1 is a prognostic biomarker associated with M2 macrophages in ovarian cancer, BMC Cancer 24 (1) (2024) 364.
[52] M.C. Bosco, Macrophage polarization: reaching across the aisle? J. Allergy Clin. Immunol. 143 (4) (2019) 1348–1350.
[53] C. Kerneur, C.E. Cano, D. Olive, Major pathways involved in macrophage polarization in cancer, Front. Immunol. 13 (2022) 1026954.
[54] B. Sheng, B. Zhao, Y. Dong, et al., Copine 1 predicts poor clinical outcomes by promoting M2 macrophage activation in ovarian cancer, Carcinogenesis 44 (10–11) (2023) 748–759.
[55] Z.H. Wang, B. Zhang, C.L. Zhang, et al., Effect of region on the outcome of patients receiving PD-1/PD-L1 inhibitors for advanced cancer, Int. Immunopharm. 74 (2019).
[56] W. Tian, N. Lei, J. Zhou, et al., Extracellular vesicles in ovarian cancer chemoresistance, metastasis, and immune evasion, Cell Death Dis. 13 (1) (2022) 64.